Proceedings of the ASME 2017 International Design Engineering Technical Conferences and Computers and Information in Engineering Conference
IDETC/CIE 2017
August 6-9, 2017, Cleveland, Ohio, USA

DETC2017-67355

DESIGN AND APPLICATION OF FRACTIONAL ORDER PIΛDM CONTROLLER IN GRID-CONNECTED INVERTER SYSTEM

Zhifeng Pan
South China University of Technology
Guangzhou, 510640, China

Xiaohong Wang
South China University of Technology
Guangzhou, 510640, China
School of Eng'g, University OF California
Merce ,CA95343， USA

Thi Thu Giang Hoang
South China University of Technology
Guangzhou, 510640, China
Thai nguyen University of Technology
Thai nguyen, Vietnam

Ying Luo
Huazhong University of Science and Technology
Wuhan, 430074, China

Yangquan Chen
School of Eng'g, University OF California
Merce,CA95343， USA

Lianfang Tian
South China University of Technology
Guangzhou, 510640, China

ABSTRACT

In comparison with the traditional controller PID, the fractional order controller $PI^{\lambda}D^{\mu}$ is added with two parameters (μ and λ), that increases the flexibility of the controller. The larger adjustable space makes it more favorable to the control of the nonlinear system like the three-phase grid-connected inverter. However, since the fractional calculus operator is an irrational function on the complex plane, it can't be implemented directly in simulation or in practical applications. In this paper, the advantages of the fractional order controller $PI^{\lambda}D^{\mu}$ will be analyzed, then the fractional calculus operator is fitted by the frequency domain analysis method. Based on the vector method, the fractional order controller $PI^{\lambda}D^{\mu}$ of the grid-connected inverter is designed. Simultaneously, the optimal controller parameters are searched with the ITAE and IAE as the performance index. And finally, the results are compared with those of the traditional controller PID. In consideration of the defects of fractional algorithm and single discretization method, a hybrid discretization method is proposed in order to ensure that the discretized controller can keep the same time-domain response and frequency characteristics as the designed controller. The experimental results show that the proposed method has the dynamic and static characteristics better than the traditional controller PID, which proves that the application of fractional order controller in three-phase grid-connected inverter is effective and feasible.

Keywords: Grid-Connected Inverter, Fractional Order, PID Controller, Discretization, Vector Method.

INTRODUCTION

Three-phase grid-connected inverter can achieve sinusoidal current, unity power factor operation, and DC-AC conversion [1], so it plays a significant role in research and application. Three-phase grid-connected inverter often uses two control loops with PID regulator [2]. Theoretically, PID controller can be used to control DC bus voltage and current-loop current without static error. Furthermore, sinusoidal current will be realized in the steady state, which is in the same phase as the phase voltage of the grid side [3]. However, there is a problem with the design of parameters that are not exactly accurate, influenced by modulation methods, the characteristics of the power switch tube and the dead time, and so on. As we have known, the three-phase inverter is highly nonlinear, so using conventional PID controllers can't achieve good control results.

To enhance the quality of control, especially the quality of the grid current, it is imperative to improve the traditional PID controller. This paper analyzes the three-phase grid-connected inverter and designs the fractional controller $PI^{\lambda}D^{\mu}$ for the current loops. Compared to conventional PID controllers, the fractional controller $PI^{\lambda}D^{\mu}$ has two additional parameters μ and λ that increase the adjustment ability of the controller, μ and λ can be selected as a decimal; therefore it is suitable for nonlinear control systems [4]. The fractional controller $PI^{\lambda}D^{\mu}$ has strong robustness, better results than conventional PID controller. At the same time, this paper also considers a method for digital algorithm and disadvantages of single discretization method, then we introduced hybrid discretization method and discretized the fractional controller $PI^{\lambda}D^{\mu}$. This hybrid discretization method can adhere to an extreme at frequency range to select suitable discretization method, with a small deviation, and ensure that the discretized controller has frequency characteristics similar to proposed controller. Finally, through simulation and testing results, we compare the control results of the conventional PID controller and the fractional controller $PI^{\lambda}D^{\mu}$, demonstrating the feasibility and superiority of the fractional controller $PI^{\lambda}D^{\mu}$.

NOMENCLATURE

1. Control of grid-connected inverter

Consider the circuit topology of three-phase grid-connected inverter in Fig. 1, where u_a, u_b, u_c are the grid side voltage; v_a, v_b, v_c are the fundamental voltage of the power devices in AC side; i_a, i_b, i_c are the grid side current with the inductor *L* for filtering and its internal resistance *R*. Moreover, I_{dc} is the DC side current, U_{dc} is the DC bus voltage, I_L is the load current, and R_L is the load. Also, *C* is the DC bus filter capacitor, and e_L stands for the possible reverse electromotive force (when the load is a generator).

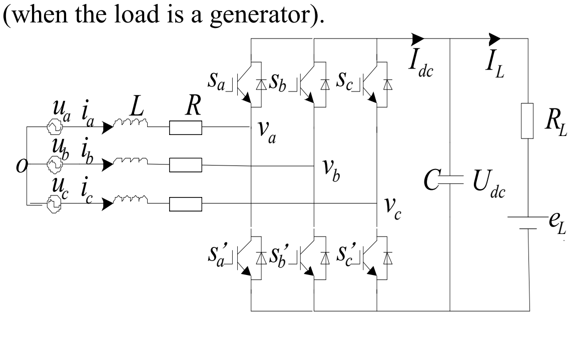

Figure 1. Circuit of three-phase grid-connected inverter

The control objectives of the three-phase grid-connected inverter are as follows: (1) to stabilize the DC bus voltage, and the dynamic response is fast; (2) to achieve sinusoidal current of the grid side, and the power factor is high. Therefore, voltage and current closed-loop method can be used to control the system. Generally, voltage loop, as the outer ring, is used to ensure the stability of the DC bus voltage. And the current loop, as the inner loop, is used to adjust the current quickly, so as to improve the speed of current control. The control diagram of three-phase grid-connected inverter is shown in Fig. 2.

In order to simplify the control of the current, feed-forward decoupling control strategy [5] is used to decouple the current in *d* axis and *q* axis. The current loop control diagram with feedforward decoupling is shown in Fig. 3, where, ω is the angular frequency of grid side voltage; u_d, u_q and i_d, i_q are components in *d* axis and *q* axis of the three-phase grid voltage and current with $3s/2r$ transformation; i_d^*, i_q^* are the set point of i_d, i_q; G_c is current regulator.

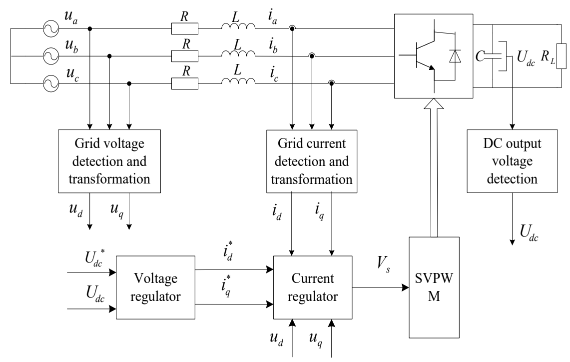

Figure 2. Control diagram of three-phase grid-connected inverter

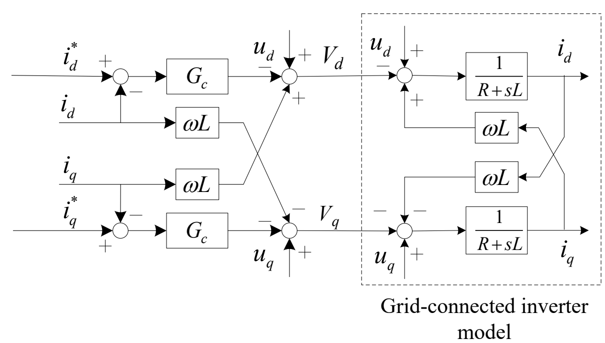

Figure 3. Current loop control diagram with feedforward decoupling

In the traditional control, the PI controller is used to regulate the voltage and current without static error. Based on the control target and the characteristics of the fractional order $PI^{\lambda}D^{\mu}$ controller, fractional order PI^{λ} controller is proposed to transform the current loop in this paper, and the voltage loop still adopts the traditional PI control.

Considering the influence of the current sampling and SVPWM method in practical application, regard each of them as a small inertia element and let the time constant be T_1, T_2. For the case of two inertia elements in series, if the condition (1) is met, the two can be combined into one.

$$\omega_c \le \frac{1}{3}\sqrt{\frac{1}{T_1 T_2}} \tag{1}$$

Where, ω_c is the open-loop cutoff frequency. Then incorporate it into the model shown in Fig. 3, we have

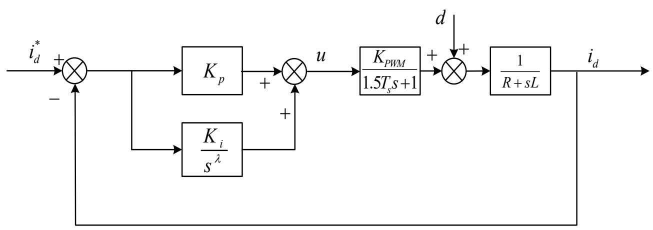

Figure 4. The actual current loop control diagram

Thus, the controlled plane of the actual current loop can be written as

$$G_o(s) = \frac{K_{pwm}}{(Ts+1)(sL+R)} \tag{2}$$

Where, K_{pwm} is the gain of modulation, $T = 1.5T_s$ and T_s is the sampling period of the grid side current as well as the switching period of IGBT.

2. Characteristics of fractional order controller

For the general control system, the structure of the fractional order $PI^{\lambda}D^{\mu}$ controller shown in Fig. 5:

The general form of the fractional order $PI^{\lambda}D^{\mu}$ controller can be written as

$$u(t) = k_p e(t) + k_i D^{-\lambda} e(t) + k_d D^{\mu} e(t) \tag{3}$$

or in transfer function form [6]

$$G_c(s) = \frac{U(s)}{E(s)} = K_p + \frac{K_i}{s^{\lambda}} + K_d s^{\mu} (0 < \lambda, \mu < 2) \tag{4}$$

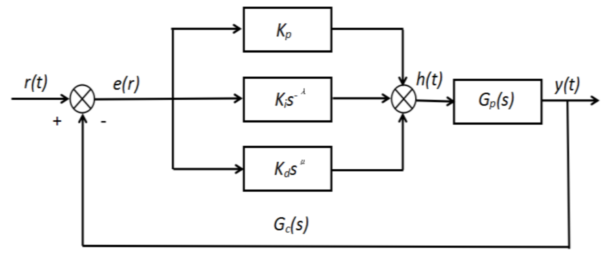

Figure 5. Control system with fractional order $PI^{\lambda}D^{\mu}$ controller

From expression (4), we can know that the fractional order $PI^{\lambda}D^{\mu}$ controller can be divided into three part: proportional, integral and differential part. Each of them has a corresponding vector in the field of complex plane. In other words, any fractional order $PI^{\lambda}D^{\mu}$ vector can be decomposed into a proportional vector, an integral vector, and a differential vector in the complex plane. Its corresponding vector model is shown in Fig. 6, where the proportional vector coincides with the real axis in the same direction and the size is the same as the value on the real axis; the integral vector is mainly distributed in the third and fourth quadrants of the complex plane, its length is $|\frac{K_i}{\omega^{\lambda}}|$ and its angle with the real axis is $\frac{\pi}{2}\lambda$; the differential vectors are mainly distributed in the first and second quadrants of the complex plane with the length $|K_d\omega^{\mu}|$ and the angle $\frac{\pi}{2}\mu$ between the vector and the real axis.

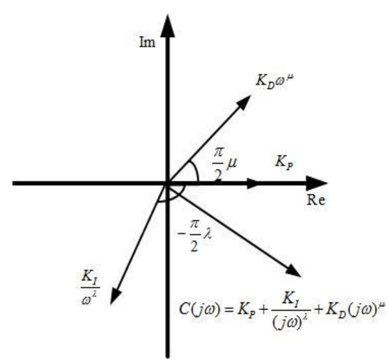

Figure 6. Schematic diagram of fractional order $PI^{\lambda}D^{\mu}$ controller vector model

It can be seen from Fig.6 that the vector of the fractional order controller $PI^{\lambda}D^{\mu}$ can represent all the vectors of the complex plane due to the existence of the fractional order μ and λ. However, the traditional PID controller can only synthesize the vectors of the first and fourth quadrants.

In a word, the fractional order controller $PI^{\lambda}D^{\mu}$ can provide a larger lead phase or lag phase. Meanwhile, for the same vector, more combinations can be chosen. Thus, the fractional order controller is more flexible and adjustable.

3. Design of fractional order PI^{λ} controller

For the controlled object $G_0(s)$ shown in expression (2), it can be represented by the vector *P* on the complex plane. Given the cutoff frequency ω_c, it is easy to get the modulus and angle of *P*.

$$\left|P(j\omega_c)\right| = \frac{K_{pwm}}{\sqrt{(T\omega_c)^2+1}\cdot\sqrt{(L\omega_c)^2+R^2}} \tag{5}$$

$$Arg[P(j\omega_c)] = -(\arctan T\omega_c + \arctan\frac{L}{R}\omega_c) \tag{6}$$

For a given index of parameters tuning, it can be expressed by the vector *G*, and consider it as the index after the correction by the controller. Given the phase margin Φ_m and the cutoff frequency ω_c, the modulus and angle of *G* should meet the following requirements:

$$\left|G(j\omega_c)\right| = 1 \tag{7}$$

$$Arg[G(j\omega_c)] = \Phi_m - 180^\circ \tag{8}$$

Define the correction vector *C* as the vector represented by the fractional order PI^{λ} controller, we know that the relationship between the vector C, P and *G* is

$$C \bullet P = G \tag{9}$$

According to the expressions (7) to (9), we have

$$C(j\omega_c) = \frac{1}{\left|P(j\omega_c)\right|} Arg[\Phi_m - Arg[P(j\omega_c)] - 180^\circ] \tag{10}$$

Let *A* be the modulus and θ be angle of the vector *C*, then

$$A = \frac{1}{\left|P(j\omega_c)\right|} = \sqrt{(T\omega)^2+1} \bullet \sqrt{(L\omega)^2+R^2} \tag{11}$$

$$\theta = \Phi_m - Arg[P(j\omega_c)] - 180^\circ \tag{12}$$

Then the vector model of the fractional order PI^{λ} correction vector *C* designed in this paper can be shown on the complex plane in Fig. 7.

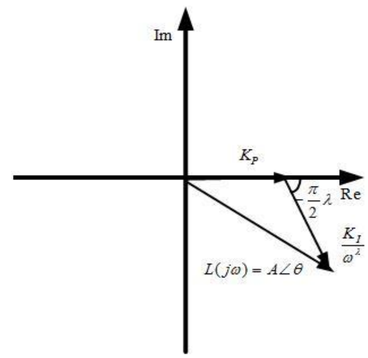

Figure 7. Fractional order PI^{λ} correction vector model

From Figure 7 the following equations can be listed according to the analysis of the trigonometric function relationship.

$$K_p + \frac{K_i}{\omega_c^{\lambda}}\cos(-\frac{\pi}{2}\lambda) = A\cos\theta \tag{13}$$

$$\frac{K_i}{\omega_c^{\lambda}}\sin(-\frac{\pi}{2}\lambda) = A\sin\theta \tag{14}$$

In the three-phase grid-connected inverter system of this paper, the switching frequency of IGBT is 10 *kHz*, so T_s can be set to 0.0001*s*. And the grid side inductance is 5*mH*, so take *L* as 0.005*H*. While *R* is the sum of the switching loss and the internal resistance of filter inductance, let *R* be 0.05*Ω*. As the dead time is 5*μs*, K_{pwm} is about 1.24. Substituting the above parameters into expression (2), the controlled plane of the actual current loop in this paper can be written as

$$G_o(s) = \frac{1.24}{7.5\times10^{-7}s^2 + (5\times10^{-3} + 7.5\times10^{-6})s + 0.05} \tag{15}$$

Let the phase margin Φ_m be 60^o. In consideration of the condition (1) of this system ($\omega_c \le 4714 rad/s$), the search range of the cutoff frequency ω_c is set to 3000 to 4000 *rad/s*. In conditions ($K_p > 0, K_i > 0, \lambda \in [0,2]$), by minimizing the index function *J*, a set of optimal parameters in the workspace is obtained. Considering the tracking performance of the system and its ability to suppress the harmonic interference, the performance criteria *J* can be chosen as

$$J = IAE + ITAE = \int_0^\infty \left|\mathrm{y(t)}\right| dt + \int_0^\infty t\left|e(\mathrm{t})\right| dt \tag{16}$$

Where, IAE stands for the integral of absolute output under harmonic interference only (d in Fig. 4), and ITAE is the integral of time multiplied by the absolute value of error with a step input only (i_d^* in Fig. 4).

For each point in the search interval, the fractional order PI^{λ} controller parameters are solved by the expression (13), (14), then parameters is put into the control system, shown in Fig. 4, to obtain the response and the index J is calculated at the same time. Finally, the J curve is plotted with the cutoff frequency ω_c and the integral order λ, so as to find out ω_c, λ and the controller parameters K_p, K_i corresponding to the minimum J. As J is too large to be taken into account when λ<0.2, ignore the data of this part then we get Fig.8.

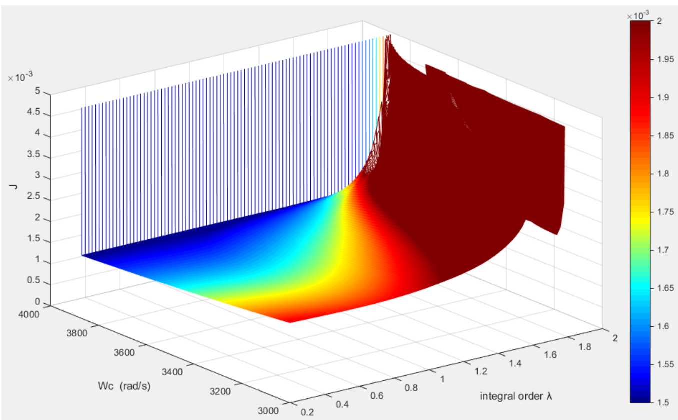

Figure 8. J with different cutoff frequency ω_c and integral order λ

From Figure 8, we find $\omega_c = 3870 rad/s$ and λ=1.34 when J is the minimum. And the corresponding controller parameters are $K_p = 18$ and $K_i = 302.67$. Thus, the fractional order PI^{λ} controller $G_c(s)$ can be written as

$$G_c(s) = 18 + \frac{302.67}{s^{1.34}} \tag{17}$$

Take the same search interval, the optimal parameters of the traditional PI controller can be also obtained.

$$G_c(s) = 18 + \frac{78.4}{s} \tag{18}$$

4. Numerical realization of fractional order operators

In order to make the fractional order controller effective in the system designed in this paper, this section will focus on the numerical implementation of fractional order controller.

In expression (4), we can find that the realization of the fractional order $PI^{\lambda}D^{\mu}$ controller is ultimately attributed to the numerical implementation of the fractional calculus operator. However, since the fractional calculus operator is an irrational function on the complex plane, it can't be implemented directly in simulation or in practical applications. Therefore, it is necessary to find a suitable method to fit the fractional calculus operator. The fitting methods usually used are as follows: power series expansion [7], continuous fraction expansion [8, 9], Carlson method [10], Matsuda's method [11], Chareff's method [11], Oustaloup's approximation [12-14], etc. In this paper, the improved optimal rational approximation (ORA) is adopted.

The optimal rational approximation method is also a practical fitting method. The main idea of this method is to set a max deviation ε of amplitude-frequency characteristic between the approximate function *R(s)* and the objective function $G_o(s)$ as a standard. Then according to this standard, the optimal approximation is achieved by limiting the error of the approximate function not to exceed the agreed range. In order to keep the amplitude-frequency characteristic consistent with its phase-frequency of the rational approximate function, a construction method can be established on the minimum phase system. The rational approximation transfer function is constructed by using n single negative real zeros and m single negative real poles, where the relationship between the number of zeros and poles is met the condition follow.

$$0 \le |n - m| \le 1 \tag{19}$$

However, as one of the high-order fitting methods, the disadvantage of the ORA method is that the low frequency gain is a finite constant. Therefore, the steady-state gain is not infinite, so the controller obtained by this method will surely lead to the static error of the control system. In order to avoid the static error, the above methods should be improved. For the fractional integral operator $\frac{1}{s^{\lambda}}(0<\lambda<1)$, we can first use the ORA method to fit the differential operator $s^{1-\lambda}$ in the approximation frequency range $[\omega_a, \omega_b]$ and then take an integral part $\frac{1}{s}$ to get the integral operator $\frac{1}{s^{\lambda}}$. In this case, the slope of the amplitude-frequency characteristic outside the approximation range is increased by -20 *dB/dec*, while maintaining the original characteristic inside the range.

Assuming that the approximation frequency range is $[\omega_a, \omega_b]$, the crossing frequency is ω_c, and the relationship between them satisfies $\omega_a < \omega_b < \omega_c$. For example, the fitting process of the fractional integral operator $\frac{1}{s^{\lambda}}(0<\lambda<1)$ used the improved ORA method is shown in Fig. 9.

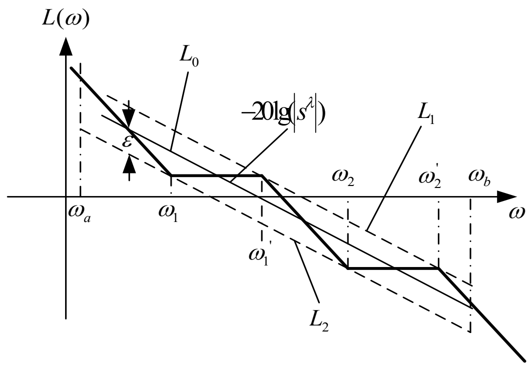

Figure 9. Schematic diagram of rational approximation

Where ω_1 can be set freely and the recurrence formulas for the turning points is

$$k_1 = 10^{\frac{\varepsilon}{20}} \tag{20}$$

$$k_2 = \frac{1}{10^{\frac{\varepsilon}{20}}} \tag{21}$$

$$\omega_i' = \left(\frac{k_1}{k_2}\right)^{\frac{1}{\lambda}} \tag{22}$$

$$\omega_{i+1} = \left(\frac{k_1}{k_2}\right)^{\frac{1}{1-\lambda}} \omega_i' \tag{23}$$

It can been proved that an approximate transfer function *R(s)* of the fractional order integral operator $G_0(s)$ can be obtained by the recurrence formulas until ω_i' *or* ω_{i+1} *is* greater than ω_b, which can be written as

$$R(s) = \frac{k_2\omega_1^{1-\lambda}}{s} \times \frac{(\frac{s}{\omega_1}+1)\cdots(\frac{s}{\omega_n}+1)}{(\frac{s}{\omega_1'}+1)\cdots(\frac{s}{\omega_m'}+1)} = \frac{b_n s^n + b_{n-1}s^{n-1} + \cdots + b_1 s + b_0}{a_m s^{m+1} + a_{m-1}s^m + \cdots + a_1 s + s} \tag{24}$$

Where, m-n= {-1, 0}.

As one of the indirect discretization methods, the improved ORA method is more suitable for the frequency domain analysis than the conventional methods, which is in favor of the design of the controller. Moreover, in comparison with Chareff's method and Oustaloup's approximation, the fractional calculus operator obtained by the improved ORA method has better fitting frequency characteristics in the range $[\omega_a, \omega_b]$. Especially, its approximation accuracy of the phase-frequency characteristics is higher both in the high frequency and low frequency areas. Bode diagrams are shown in Fig. 10, 11, 12, where the approximation frequency range is $[10^{-6}, 10^{5}]$ and the approximate order is the same; the dashed line corresponds to the frequency characteristics using Oustaloup's approximation method and the solid line corresponds to the frequency characteristics using the improved ORA method.

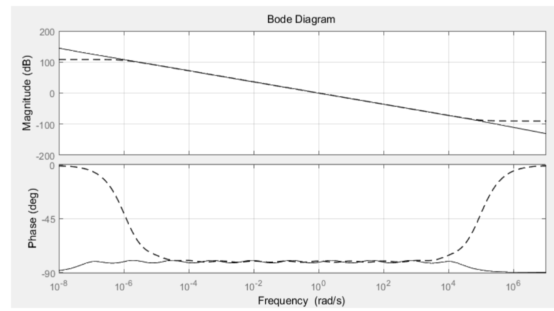

Figure 10. Comparison curves using Oustaloup's approximation and ORA (λ=0.9)

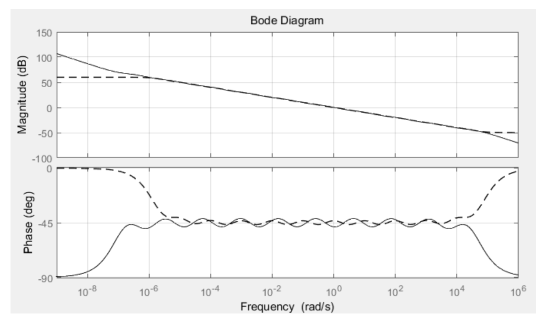

Figure 11. Comparison curves using Oustaloup's approximation and ORA (λ=0.5)

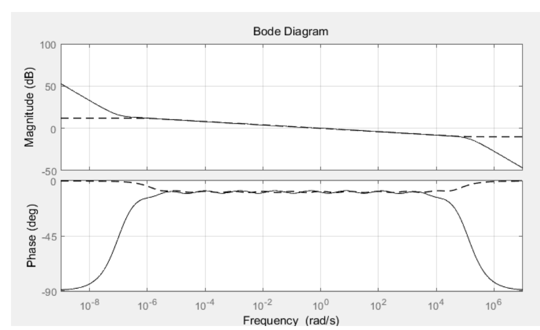

Figure 12. Comparison curves using Oustaloup's approximation and ORA (λ=0.1)

5. Discretization of fractional order PI^{λ} controller

Since the approximation function *R(s)* of the fractional order integral operator behaves as a high-order fraction, the transfer function of the fractional order PI^{λ} controller $G_c(s)$ in the frequency domain is also a high-order fraction, which can be written as

$$G_c(s) = K_p + K_i \times R(s) = \frac{b'_m s^{m+1} + b'_m s^m + \cdots + b'_1 s + b'_0}{a_m s^{m+1} + a_{m-1} s^m + \cdots + a_1 s + s} \quad (25)$$

Considering the principle of the ORA method, we know that the rational approximation function *R(s)* of the fractional integral has no repeated roots neither the zeros nor the poles. Therefore, *R(s)* can be expanded into the following form by partial fraction method.

$$R(s) = \frac{d_0}{s} + \frac{d_1}{s+\omega_1} + \frac{d_2}{s+\omega_2} + \cdots + \frac{d_m}{s+\omega_m} + k \quad (26)$$

Also, the fractional order PI^{λ} controller $G_c(s)$ can be expanded to a similar form by partial fractional methods.

$$G_c(s) = K_p + K_i \times R(s) = \frac{K_i d_0}{s} + \frac{K_i d_1}{s+\omega_1} + \frac{K_i d_2}{s+\omega_2} + \cdots + \frac{K_i d_m}{s+\omega_m} + K_i k + K_p \quad (27)$$

In this paper, a hybrid discretization method is proposed in order to ensure that the discretized controller $G_c(s)$ can keep the same time-domain response and frequency characteristics as the designed PI^{λ} controller $G_c(s)$. According to the characteristics of different discretization methods [15], the hybrid discretization method uses impulse response method or bilinear transformation method in different frequency range for Z transform, in order to combine the advantages of this two methods and make it better.

The main idea of compound Z transform is: firstly, $G_c(s)$ is expanded by partial fraction method, then a frequency threshold is set based on the sampling frequency ω_s (here we choose $\omega_s / 3$), and judge whether the poles of each link is greater than the threshold. If it is, use bilinear transformation method, otherwise, the Z transform is carried out by impulse response method. Finally, the discrete realization $G_c(z)$ of the fractional order PI^{λ} controller is obtained by adding all the Z-transformed fractions. The design idea is shown in the following diagram, where ω_m is greater than the threshold, and ω_1 is less than the threshold.

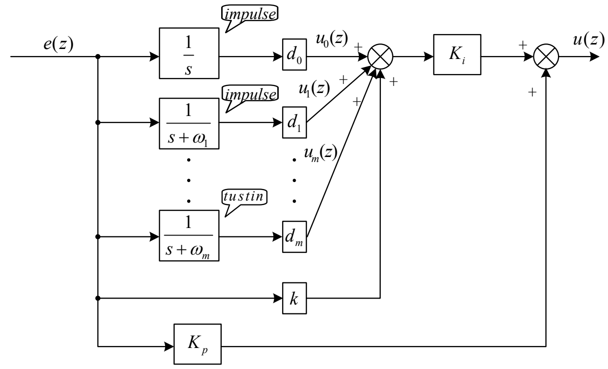

Figure 13. Design block diagram of the hybrid discretization method

The advantage of this discretization method is that it divides a high-order transfer function into the form of multiple first-order transfer functions in parallel, and combines the advantages of different discretization methods to select the better one according to the different frequency range of the poles. At the same time, when the first-order transfer function is discretized, the operation precision is high, so that it is easy to avoid the distortion caused by insufficient high-order operation precision. Moreover, the number of points that need to be stored in the past is relatively smaller in digital implementation.

The comparison curve between the continuous controller $G_c(s)$ and the discrete controller $G_c(z)$ is as shown in Fig. 14. It can be seen that the output of the discrete controller $G_c(z)$ is very close to the output of the continuous controller $G_c(s)$, with a small error. Thus, the effectiveness of this method is proved.

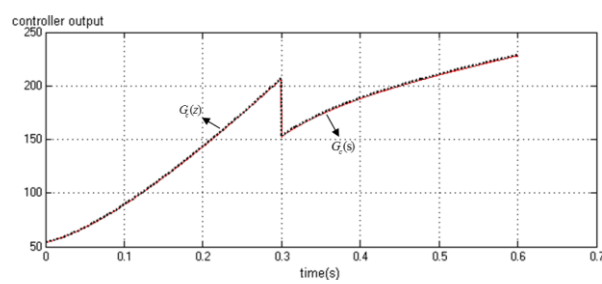

Figure 14. Step response of continuous controller $G_c(s)$ and discrete controller $G_c(z)$

6. Simulation and experimental results

In order to compare the control effect of traditional PI controller and fractional order PI^{λ} controller, some corresponding simulations and experiments are carried out.

- **Simulation:**

In the three-phase grid-connected inverter simulation system, the DC bus voltage is set to 660V, the dynamic and static voltage, current and the total harmonic distortion (THD) of the system with load are shown as follows, where the load is suddenly changed in the intermediate instant.

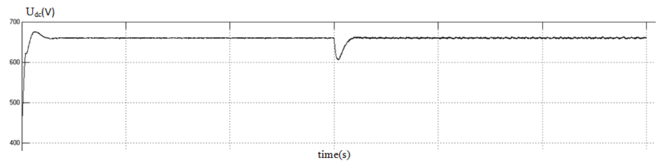

Figure 15. The DC bus voltage of the closed-loop system with the traditional PI controller

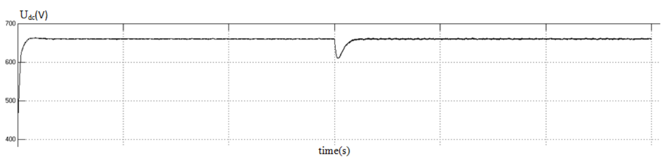

Figure 16. The DC bus voltage of the closed-loop system with the fractional order PI^{λ} controller

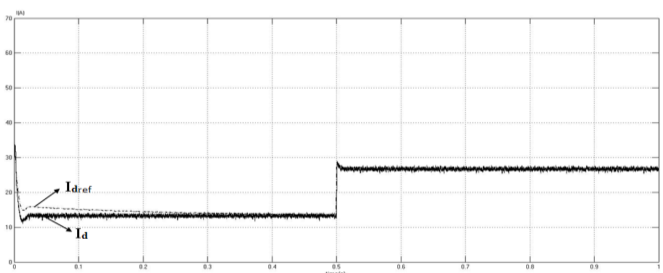

Figure 17. The active current I_d of the closed-loop system with the traditional PI controller

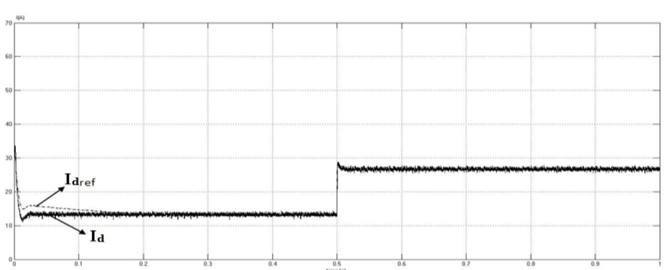

Figure 18. The active current I_d of the closed-loop system with the fractional order PI^{λ} controller

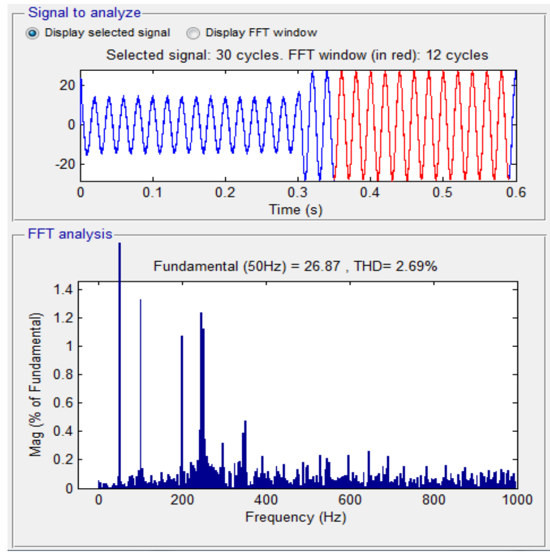

Figure 19. The grid side current i_a and its *THD* of the closed-loop system with the traditional PI controller

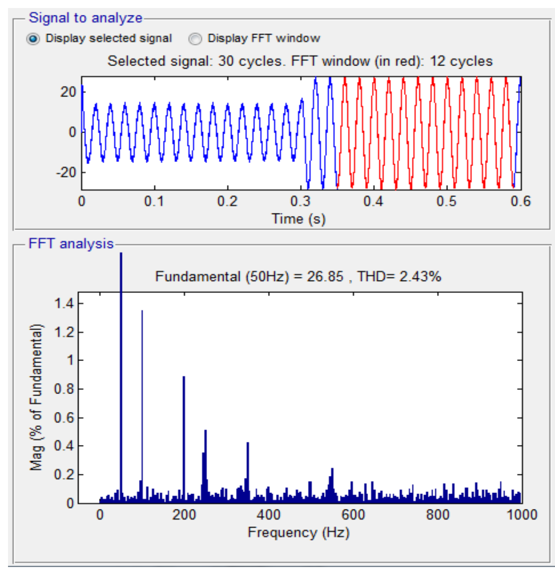

Figure 20. The grid side current i_a and its *THD* of the closed-loop system with the fractional order PI^{λ} controller

Comparing Figure 15 with Figure16, it can be seen that the DC bus voltage of the closed-loop system with the fractional order controller PI^{λ} increases faster, with smaller overshoot, shorter settling time. Furthermore, the drop is smaller and the time returning to steady state is shorter when the load is suddenly changed in the intermediate instant.

From Figure 17 and Figure 18, we know that the active current I_d of the closed-loop system with the fractional order controller PI^{λ} is slightly overshooting but its settling time is evidently shorter. And under the influence of the sudden load, the active current I_d also rises faster and more stable.

As for Figure 19 and Figure 20, it can be found that the grid side current of the closed-loop system with each controller has excellent sinusoidal and low harmonic distortion THD. However, the THD by the effect of the fractional order controller PI^{λ} is 2.43%, which is less than the THD (2.69%) under the action of the traditional controller PI.

- **Analyze the experiments at the static state:**

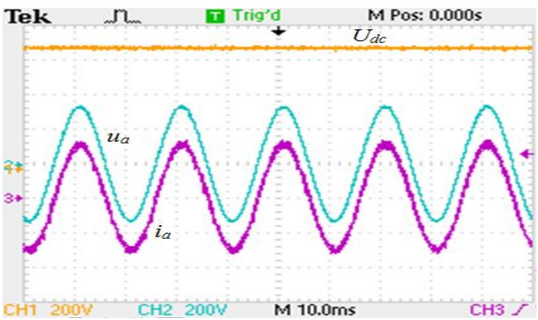

Figure 21. Voltage and current characteristics of the inverter when using PI controller with 6KW load capacity

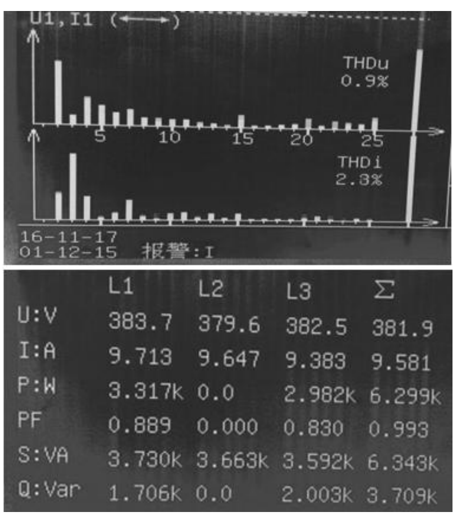

Figure 22. Experiment parameters when using PI controller and operating with 6KW load capacity

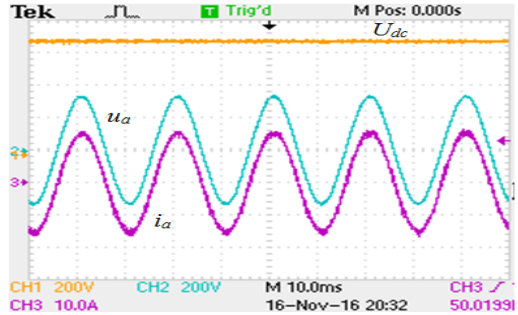

Figure 23. voltage and current characteristics of the inverter when using PI^{λ} controller 6KW controller with 6KW load capacity

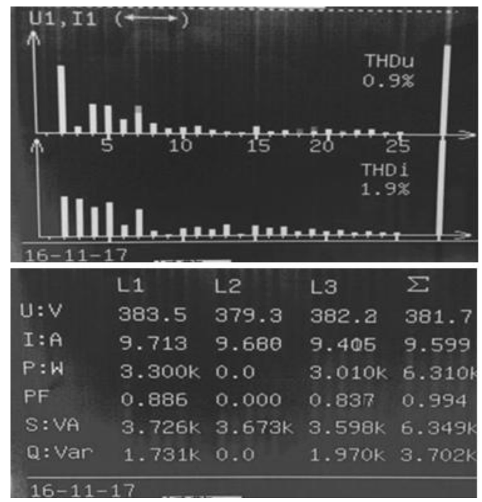

Figure 24. Experiment parameters when using PI^{λ} controller and operating with 6KW load capacity

Comparison of Figures 21 and 23 shows that, when the system is operating at a constant load of 6KW, voltage and current are in phase, basic control objective of unity power factor is obtained. But it can also be seen that, when operating in steady state, under the effect of the fractional controller PI^{λ}, the current in the grid is more sinusoidal.

According to the parameters in Figure 22 and Figure 24, the analysis and comparison of the two conventional controller PI and the fractional order controller PI^{λ} in static state, is not much different of power factors between both controllers, under the influence of controller PI, the total harmonic distortion is 2.3%, while using fractional controller PI^{λ} the total harmonic distortion is 1.9%. It can be seen that using fractional order controller PI^{λ} has better harmoic inhibilation .

- **Analyze the results of experiments when the load changes:**

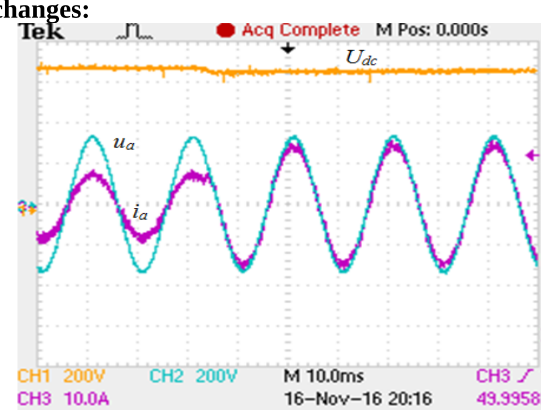

Figure 25. The voltage and current characteristics of the inverter when using the PI controller and changing the loa

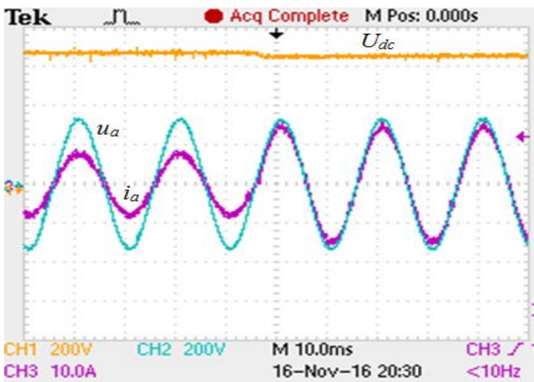

Figure 26. The voltage and current characteristics of the inverter when using the fractional controller PI^{λ} and changing the load

After the system has operated for some time, we increase the load capacity from 3KW to 6KW. From Figure 25 and Figure 26 it can be seen that, when using the PI controller, the phase current adjusts to the sinusoidal waveform after a period of less than half cycle, while using the fractional order controller PI^{λ}, the phase current of the rectifier is not affected by changing the load, still maintain good sinusoidal ideal shape. It can easily be seen that, under the influence of the two controllers, the current and the voltage are both in phase, the grid inverters obtain the purpose of unity power factor.

Thus, the results show that when using conventional controller PI and fractional order controller PI^{λ}, with different load capacities, analysis and comparison in both static and dynamic state, it can be proved that the use of fractional order controller PI^{λ} to control the three-phase grid-connected inverter provides better results, the application of fractional controller in this system is feasible and effective.

7. Conclusion

In the three-phase grid-connected inverter system, a fractional order controller PI^{λ} is designed based on the frequency domain analysis method. Under the same conditions, the parameters of the fractional order controller PI^{λ} and the traditional controller PI are adjusted separately. Considering the digital realization of the fractional order controller, a hybrid discretization method is proposed in order to ensure that the discretized controller can keep the same time-domain response and frequency characteristics as the designed controller.

With a series of simulations and experiments, it is proved that the fractional order controller PI^{λ} can play a good role in the control. And the dynamic and steady-state performance with the fractional order controller PI^{λ} are better than those with the traditional controller PI. Therefore, the application of the fractional order controller PI^{λ} in this system is feasible and effective. Moreover, the fractional order controller PI^{λ} has more flexibility than the traditional controller PI. Therefore, its further application is very promising.

ACKNOWLEDGMENTS

This work as supported by the Project of Guangdong Province，China No.2015A010106004； 2016B090911003; the Project of Guangzhou city ,China,No. 201508030040.

REFERENCES

[1] Wang Y, Yan Z, Zhang Z, et al. A New PI Algorithm for Single Stage Three-Phase Grid-Connected Photovoltaic Inverter Based on Power Feed-Forward[C]//Instrumentation and Measurement, Computer, Communication and Control (IMCCC), 2015 Fifth International Conference on. IEEE, 2015: 1025-1030.

[2] Tsengenes G, Adamidis G. Comparative evaluation of fuzzy-PI and PI control methods for a three phase grid connected inverter[C]//Power Electronics and Applications (EPE 2011), Proceedings of the 2011-14th European Conference on. IEEE, 2011: 1-10.

[3] Windarko N A, Qudsi O A, Tjahjono A, et al. Optimized PI constant for current controller of grid connected inverter with LCL filter using Genetic Algorithm[C]//Electrical Engineering and Informatics (MICEEI), 2014 Makassar International Conference on. IEEE, 2014: 9-13.

[4] Marshiana D, Thirusakthimurugan P. Fractional order PI controller for nonlinear systems[C]//Control, Instrumentation, Communication and Computational Technologies (ICCICCT), 2014 International Conference

on. IEEE, 2014: 322-326.

[5] Huang T, Shi X, Sun Y, et al. Three-phase photovoltaic grid-connected inverter based on feedforward decoupling control[C]//Materials for Renewable Energy and Environment (ICMREE), 2013 International Conference on. IEEE, 2014, 2: 476-480.

[6] Shah P, Agashe S D, Singh A P. Design of fractional order controller for undamped control system[C]//Engineering (NUiCONE), 2013 Nirma University International Conference on. IEEE, 2013: 1-5.

[7] Chen Y Q, Moore K L. Discretization schemes for fractional-order differentiators and integrators[J]. IEEE Transactions on Circuits and Systems I: Fundamental Theory and Applications, 2002, 49(3): 363-367.

[8] Chen Y Q, Vinagre B M, Podlubny I. Continued fraction expansion approaches to discretizing fractional order derivatives—an expository review[J]. Nonlinear Dynamics, 2004, 38(1): 155-170.

[9] Singh K J, Mehra R, Pal G P. Improved design of IIR-type digital fractional-order differentiators using continuous fraction expansion[C]//Recent Advances in Engineering & Computational Sciences (RAECS), 2015 2nd International Conference on. IEEE, 2015: 1-5.

[10] Shrivastava N, Varshney P. Rational approximation of fractional order systems using Carlson method[C]//Soft Computing Techniques and Implementations (ICSCTI), 2015 International Conference on. IEEE, 2015: 76-80.

[11] Vinagre B M, Podlubny I, Hernandez A, et al. Some approximations of fractional order operators used in control theory and applications[J]. Fractional calculus and applied analysis, 2000, 3(3): 231-248.

[12] Xue D, Zhao C, Chen Y Q. A modified approximation method of fractional order system[C]//Mechatronics and Automation, Proceedings of the 2006 IEEE International Conference on. IEEE, 2006: 1043-1048.

[13] Oustaloup A, Levron F, Mathieu B, et al. Frequency-band complex noninteger differentiator: characterization and synthesis[J]. IEEE Transactions on Circuits and Systems I: Fundamental Theory and Applications, 2000, 47(1): 25-39.

[14] Khanra M, Pal J, Biswas K. Rational approximation of fractional operator—A comparative study[C]//Power, Control and Embedded Systems (ICPCES), 2010 International Conference on. IEEE, 2010: 1-5.

[15] Zhao H, Wang Z, Jia H. Comparison and Analysis of Discretization Methods for Continuous Systems[J]. Indusrty and Information Technology Education, 2015 (10): 71-76.

[16] Xu H, Li G, Huang C. A novel approach to stable IIR digital filter design[C]//Information, Communications and Signal Processing, 2009. ICICS 2009. 7th International Conference on. IEEE, 2009: 1-5.

[17] Monje C A, Chen Y Q, Vinagre B M, et al. Fractional-order systems and controls: fundamentals and applications[M]. Springer Science & Business Media, 2010.

[18] Ang G, Jianru W, Zhiwei N, et al. Research on current feed forward decoupling control for energy feedback and grid-connected device[C]//Power Electronics Systems and Applications (PESA), 2011 4th International Conference on. IEEE, 2011: 1-6.

[19] Chen Y Q, Moore K L. Discretization schemes for fractional-order differentiators and integrators[J]. IEEE Transactions on Circuits and Systems I: Fundamental Theory and Applications, 2002, 49(3): 363-367.

[20] Lar I, Radulescu M M, Ritchie E, et al. Current control methods for grid-side three-phase PWM voltage-source inverter in distributed generation systems[C]//Optimization of Electrical and Electronic Equipment (OPTIM), 2012 13th International Conference on. IEEE, 2012: 859-867.